Corrosion suppression of aluminium current collectors within Li-ion cells using 3-methoxypropionitrile-based electrolytes

Chih-Han Yen [a,b], Alex R. Neale [b], Jungwoo Lim [b,c], Dominic Bresser [d,e], Laurence J. Hardwick [b,c,*], Chi-Chang Hu [a,*]

[a] Department of Chemical Engineering, National Tsing Hua University, Hsinchu 300044, Taiwan
[b] Department of Chemistry, Stephenson Institute for Renewable Energy, University of Liverpool, Liverpool L69 7ZD, UK
[c] The Faraday Institution, Harwell Campus, Didcot OX11 0RA, UK
[d] Helmholtz Institute Ulm (HIU), Ulm 89081, Germany
[e] Karlsruhe Institute of Technology (KIT), Karlsruhe 76021, Germany

A B S T R A C T

Electrolytes containing lithium bis(trifluoromethylsulfonyl)imide (LiTFSI) as the conductive salt generally possess the high moisture tolerance and innate HF-free generation in moisture environments in comparison with those containing lithium hexafluorophosphate ($LiPF_6$). However, severe corrosion of the aluminium current collector presently hinders the use of LiTFSI within Li-ion cells. Here 3-methoxypropionitrile (MPN) is introduced as an alternative, non-toxic solvent into the electrolyte formulation to explore the effects on Al corrosion. The MPN-containing electrolytes can suppress Al corrosion via the generation of an aluminium nitride dominated protection layer during charge-discharge cycling, as confirmed by X-ray photoelectron spectroscopy. For the cycling performance of Li||$LiNi_{0.6}Mn_{0.2}Co_{0.2}O_2$ half cells, the increasing addition of MPN solvent improves capacity retention and suppresses the corrosion of Al current collectors in LiTFSI containing electrolytes.

1. Introduction

Lithium-ion cell technology has dominated the portable electronics industry and has made strong inroads as the energy storage system of choice for electric vehicles and parts of the electricity grid [1–6]. Conventional lithium-ion cell electrolytes are based on lithium hexafluorophosphate ($LiPF_6$) and possess high ionic conductivity and good electrochemical stability. However, $LiPF_6$ readily reacts with moisture impurities in the electrolyte to generate hydrogen fluoride (HF) [7] and the reaction onset temperature is ca. 27°C [8]. HF attacks the surface of the positive electrode and accelerates the dissolution of transition metals, resulting in poor performance of various positive electrode materials [9,10]. Furthermore, the thermal decomposition temperature of pure $LiPF_6$ salt in dry inert atmosphere is up to 107°C however, this value decreases to 87°C in the presence of water. Therefore, several alternative salts have been developed, and lithium bis(trifluoromethylsulfonyl)imide ($LiC_2F_6NO_4S_2$, LiTFSI) is a promising candidate for the replacement of $LiPF_6$ because it has a high thermal decomposition temperature of 340°C [11], excellent moisture stability [12], long-term stability at various pH values [12], and innate HF-free generation. Nevertheless, the utilisation of LiTFSI leads to severe corrosion of the aluminium current collectors in Li-ion cells due to the formation of soluble $Al(TFSI)_3$ as the cell potential is taken above 3.8 V *vs.* Li^+/Li [13].

Many studies on the use of electrolytes containing [TFSI] have discussed the anodic corrosion behaviour of Al current collectors [14–16]. Primarily, studies have focused on the utilisation of nitrile-based solvents to improve the stability of Al current collectors at high voltages [17–20]. Nitrile solvents have shown great potential to inhibit battery side reactions since many candidate nitrile solvents exhibit good thermal stabilities and wide electrochemical stability windows [21]. For example, the corrosion behaviour of Al can be greatly improved in the presence of adiponitrile (ADN) solvent in LiTFSI electrolytes [22]. Moreover, the physical properties of 3-methoxypropionitrile (MPN) offer superior safety in comparison with DEC (diethyl carbonate) and DMC (dimethyl carbonate). The boiling point and flashpoint of MPN are 165°C and 66°C, respectively, which are higher than those of DMC (90°C and 16°C, respectively) and DEC (127°C and 33°C, respectively) [23,24]. MPN has a low toxicity (in contrast to ADN and pimelonitrile) and, furthermore, an MPN solvent-based electrolyte can support fast charge transfer processes compared with carbonate solvents [25]. In addition, MPN has the advantages of a low melting

* Corresponding authors.
E-mail addresses: hardwick@liverpool.ac.uk (L.J. Hardwick), cchu@che.nthu.edu.tw (C.-C. Hu).

point and a high flash point; the former property is suitable for the low temperature working environments and the later one improves the safety of electrolytes [23]. The use of MPN solvent to inhibit aluminium corrosion in Li-ion batteries, however, has not been fully investigated. Herein, MPN solvent is introduced into an electrolyte containing LiTFSI as the conductive salt to enhance Al stability under high voltage operation, leading to the improvement in Li-ion cell cycling.

2. Experimental section

2.1. Electrolyte preparation

Lithium bis(trifluoromethane)sulfonimide (LiTFSI, 99.95%), diethyl carbonate (DEC, anhydrous ≥99%), dimethyl carbonate (DMC, anhydrous, ≥99%), and 3-methoxypropionitrile (MPN, 99%) (Sigma-Aldrich) and ethylene carbonate (EC, >99%) (Echo Chemical) were used to prepare the electrolytes. LiTFSI was vacuum dried in a Buchi oven at 150 °C for 3 days. MPN solvent was dried over freshly activated molecular sieves (3 Å) for 7 days before use. The 1 M LiTFSI electrolytes were prepared in an Ar-filled glovebox (H_2O, O_2 <0.1 ppm) by dissolving an appropriate amount of LiTFSI salt in solvents, which include pure EC, a mixture of EC:MPN (3:7, 1:1, and 7:3 volume ratios), and a mixture of EC:DEC (1:1 v/v). The water content of the electrolytes, checked by Karl Fischer titration, was found to be <20 ppm.

2.2. Electrode preparation

Aluminium foils (Advent Research Materials, 99.5%) were rinsed with acetone and dried in an incubator at 50°C for 1 h. Al foils were cut into 1 cm × 10 cm sheets for the corrosion tests in the electrochemical cells or punched into disk electrodes with a diameter of 12 mm for the coin cell testing. $LiNi_{0.6}Mn_{0.2}Co_{0.2}O_2$ electrodes consisted of 80 wt% $LiNi_{0.6}Mn_{0.2}Co_{0.2}O_2$ (MSE Supplies LLC), 10 wt% polyvinylidene fluoride (PVDF-Kynar®) and 10 wt% carbon black (Super C65, TIMCAL). The $LiNi_{0.6}Mn_{0.2}Co_{0.2}O_2$ slurry was coated onto Al current collectors (thickness 0.05mm, Advent Research Materials Ltd) by a doctor blade and dried initially at 60°C. 12 mm diameter $LiNi_{0.6}Mn_{0.2}Co_{0.2}O_2$ electrode discs were punched and dried under vacuum at 120°C in a Buchi oven (Buchi Labortechnik AG) for 18 h. The electrodes had an average active material loading of 5.8 mg cm^{-2} $LiNi_{0.6}Mn_{0.2}Co_{0.2}O_2$.

2.3. Electrochemical analysis

A three-electrode beaker-type cell is used to determine the onset potential of Al corrosion in various electrolytes in an Ar-filled glovebox. The Al foil (15 μm in thickness, Shining Energy) was used as the working electrode and two lithium foils (Sigma-Aldrich) served as the reference and counter electrodes. The exposed surface area of the working electrode was 1 cm^2. The anodic stability of Al foils was determined by linear sweep voltammetry (LSV) at a scan rate of 0.1 mV s^{-1} via an electrochemical analyser (CHI 6273, CH Instruments) at room temperature. The potential window of LSV was from the open-circuit potential (E_{OCP}) to 4.5 V (*vs.* Li^+/Li). The flash point of electrolytes was measured using a flash point analyser (HFP 360 Pensky-Marten, Walter Herzog GmbH, Germany).

Cell cycling tests were carried out in a $LiNi_{0.6}Mn_{0.2}Co_{0.2}O_2$ / Li coin cell using a battery tester (Maccor Series 4000). In the coin cell, the $LiNi_{0.6}Mn_{0.2}Co_{0.2}O_2$ electrode and Li metal electrode were separated by a glass fibre (Whatman® GF/F) separator wetted with the selected electrolyte (80 μL). In the coin cell cycling test, a constant dis-/charge rate of 0.5C was used to cycle the coin cell in the range of 3.0 V–4.3 V at 25°C. A 1C rate can be defined as the discharge or charge current needed to discharge or charge the entire battery capacity in 1 h.

The Arrhenius plot of ionic conductivity for various electrolytes was obtained by a conductometer (MMates Biologic) equipped with a frequency analyser and a refrigerated/heating circulator for temperature control. The electrolyte was sealed in a glass conductivity cell (assembled in the glovebox) equipped with two platinized-platinum electrodes. The ionic conductivity was measured in the temperature range from -30°C to 80°C and recorded every 5°C.

2.4. Electrode characterisation

The Al corrosion tests were conducted in coin cells, assembled with Al foil as the working electrode and Li metal as the counter electrode, separated by a glass fibre microfilter (Whatman® GF/C) separator wetted with 80 μL selected electrolyte. The working electrode was scanned to either 4.5 V or 5.0 V at a scan rate of 1 mV s^{-1} and held at the selected upper voltage limit for 10,000 s. Finally, the coin cell was disassembled, and the remaining mass of the Al foils was determined after cleaning with acetone.

X-ray photoelectron spectroscopy (XPS) was used to characterise the aluminium foils after one charge-discharge cycle from 3.0 V to 4.3 V in Al||Li coin cell with 1 M LiTFSI electrolytes using various solvents. The XPS spectra were collected using an Ar^+ beam for etching the sample. All the spectra were calibrated based on the C-C bonding at 284.5 eV. The peaks were fitted using Voigt functions after checking Shirley-type background [26].

3. Results and discussion

3.1. Electrolyte characterisation

The flash point is an important safety parameter for battery electrolytes and a comparison of the flash points of various electrolytes is shown in Table 1. The flash point temperature of the EC:MPN (1:1 v/v) solvent mixture was determined to be 84.5°C, which is higher than 36 °C, 32°C, and 25°C of the traditional mixtures containing EC:DEC (3:7 v/v), EC:EMC (1:1 w/w) and EC:DMC (1:1 w/w), respectively. The vapour pressure of ADN is three orders of magnitude lower than that of DEC and has been investigated as a high flash point co-solvent with ethylene carbonate, as shown in Table 1.

The ionic conductivities of 1 M $LiPF_6$ in EC:DMC (1:1 v/v) and 1 M LiTFSI electrolytes in EC, MPN, and EC-MPN solvents were compared in Fig. 1. Note that at temperatures higher than -10°C, the $LiPF_6$-EC:DMC electrolyte exhibits a higher conductivity than all LiTFSI-based electrolytes. On the other hand, the ionic conductivities of the MPN-enriched electrolytes become higher than that of $LiPF_6$-EC:DMC in the low temperature region (≤ -20°C). Thus, the LiTFSI-EC:MPN electrolytes with MPN ≥ 50 v% provides an additional benefit of a wider temperature working window than the $LiPF_6$-EC/DMC electrolyte.

The appropriate working voltage of Li-based batteries depends on the oxidation-reduction potentials of the electrode material, as well as the electrochemical stability of the electrolyte, electrodes and separator. Whenever Li-based batteries are developed for high-voltage (> 4 V *vs.*

Table 1
Physical properties of EC, DEC, ADN and MPN solvents. T_m melting point [27]; T_b boiling point [27]; T_f flash point [28]; η viscosity; ε dielectric constant [27].

Solvent	T_m (°C)	T_b (°C)	T_f (°C)	Vapour pressure (kPa) [28]	Viscosity η (mPa s)	Dielectric constant, ε
EC	36	238	146	0.0013 (20°C)	1.9 (40°C)	90 (40°C)
DEC	-74	127	33	2.4	0.75	2.8
DMC	5	90	16	8.0	0.59	3.1
ADN	2	295	165	0.00027	6.0	30
MPN	-57	165	66	0.23 (30°C)	1.1	36

Mixed Solvent	Flash point T_f (°C)
EC:DMC (1:1 w/w)	25 [24]
EC:EMC (1:1 w/w)	32 [24]
EC:DEC (3:7 w/w)	36 [29]
EC:ADN (1:1 w/w)	149 [29]
EC:MPN (1:1 v/v)	84.5 (Our work)

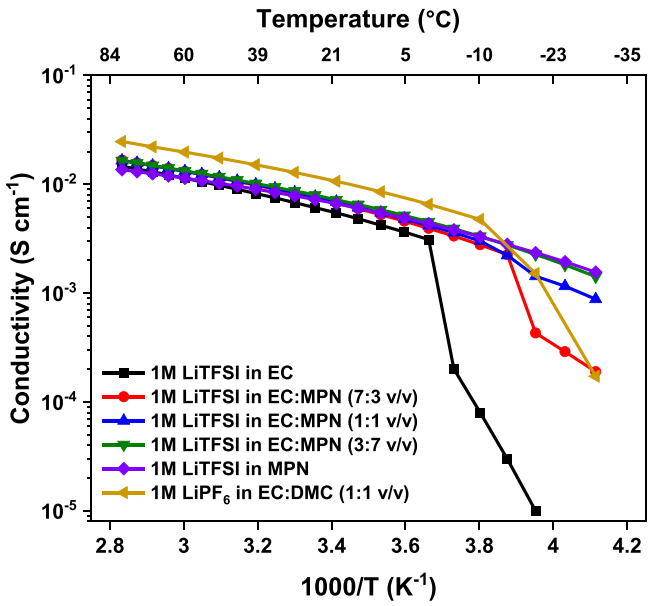

Fig. 1. Arrhenius plot of ionic conductivity of 1 M $LiPF_6$/(EC:DMC 1:1 v/v) electrolyte and 1 M LiTFSI electrolytes in various volume ratios of EC:MPN.

Li^+/Li) operation to achieve high energy densities, the influence of electrolyte composition on the stability of the Al current collector needs to be considered. Accordingly, the electrochemical stability of Al was tested in various designed electrolytes and Fig. 2 shows the linear sweep voltammetry (LSV) of Al foil electrodes in the studied series of 1 M LiTFSI electrolytes: EC, EC:MPN (7:3 v/v), EC:MPN (1:1 v/v), EC:MPN (3:7 v/v), and MPN.

In Fig. 2, the onset potential, determined by taking the linear extrapolation of the current between 10 μA cm^{-2} and 100 μA cm^{-2} to the point of intersection with the baseline current, was approximately 3.67 V (*vs.* Li^+/Li^+) in the 1 M LiTFSI/EC electrolyte which can be attributed to the Al corrosion process [14]. With an increase of MPN content in the LiTFSI electrolytes, the onset potential of Al corrosion was shifted from 3.67 V to 4.21 V (*vs.* Li^+/Li). Accordingly, the addition of MPN in the EC-based electrolytes significantly promotes the stability of the Al interface at higher voltages.

In Al||Li coin cells, the Al corrosion test was completed in various

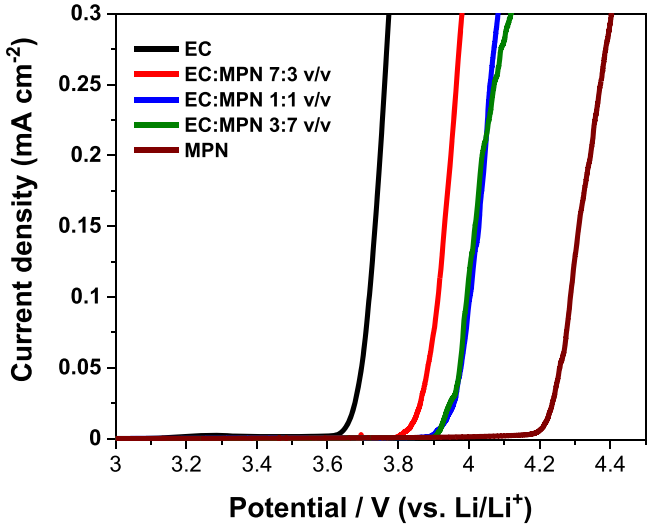

Fig. 2. Linear sweep voltammograms of Al foils in Al||Li cells measured in 1 M LiTFSI electrolytes with pure EC solvent, EC:MPN 7:3 v/v, EC:MPN 1:1 v/v, EC:MPN 3:7 v/v, and pure MPN solvent at a scan rate of 0.1 mV s^{-1}.

electrolytes using the LSV method scanning from the open-circuit potential to either 4.5 V or 5 V (*vs.* Li^+/Li^+) at a scan rate of 1 mV s^{-1} and then held at the final voltage for 10,000 s. After this corrosion test, the mass loss of the Al foils was summarized in Table 2. Obviously, the mass losses from Al corrosion are most significant in the EC electrolyte at both 4.5 V and 5 V. However, for all the electrolytes containing MPN, the Al corrosion has been effectively prohibited, even for the EC:MPN (7:3 v/v) electrolyte when the test was conducted at 4.5 V. A comparison of the data obtained at 5.0 and 4.5 V reveals that the positive effect of MPN amount in the electrolytes is visible even when the corrosion test was conducted at 5 V.

The photographic images of the foils after the 5 V corrosion test are shown in Fig. 3. Significant pitting and pores could be observed on the Al surface in the 1.0 M LiTFSI electrolyte using EC:DEC or EC solvents (see Fig. 3**(a)** and Fig. 3**(b)**), and concurs with a previous study [30]. However, the addition/substitution of MPN as solvent into the electrolyte effectively suppressed the Al corrosion, and reduced the mass loss from 18.2% in pure EC solvent to 15.3% (EC:MPN 7:3 v/v), 12.9% (EC:MPN 1:1 v/v), 8.8% (EC:MPN 3:7 v/v) and 0.5% using only the MPN solvent (Fig. 3**(c)** to Fig. 3**(f)**).

3.2. *Surface analysis by X-ray photoelectron spectroscopy*

In order to understand the chemical basis for the observed variation in corrosion and the stability afforded by the presence of MPN, X-ray photoelectron spectroscopy (XPS) was undertaken and the resulting spectra are presented in Figs. 4–6. Fig. 4 shows the XPS spectra of the Al 2p signal on the surface of Al foil after one charge-discharge cycle in the Al||Li coin cells using 1 M LiTFSI electrolytes with either EC or MPN solvent. Al 2p signals were assigned as originating from aluminium oxide and aluminium metal when using 1 M LiTFSI electrolyte with only EC solvent, as shown in Fig. 4**(a)**. The spectrum in Fig. 4**(a)** presents the top surface of Al foil contained the aluminium oxide (Al_2O_3) signal at 74.7 eV, and the metallic Al 2p signal was found to be in agreement with Al $2p_{3/2}$ at 71.6 eV and Al $2p_{1/2}$ at 72.1 eV [31,32]. Binding energy shifts observed between 0 and 30 s originates from the Ar^+ bombardment to remove surface contaminants and are associated with the surface core-level shift [33,34]. Ar^+ sputtering times of 10, 20, and 30 s were applied, which remove organic species and surface contaminants from the Al foil surface. After sputtering, the Al_2O_3 signal was measured at a consistent binding energy of 75.8 eV and the relative amount of Al $2p_{3/2}$ and Al $2p_{1/2}$ (measured at 73.3 eV and at 73.7 eV, respectively) grew with increased the sputtering time. In comparison to the EC-based formulation, the 1 M LiTFSI electrolyte with MPN solvent forms a distinctive aluminum nitride (AlN) layer on the Al surface, as shown in Fig. 4**(b)** and corroborated by N1s XPS spectra shown in Fig. 5. AlN was characterised by a binding energy of 73.5 eV on the initial Al surface and 74.4 eV after sputtering. Al_2O_3 and AlF_3 signals measured at 75.8 eV and 77.5 eV, appear at the higher signal intensity with increasing sputtering.

The N 1s XPS spectra indicate the main difference on the Al surfaces when using LiTFSI electrolyte with EC or MPN solvents, as shown in Fig. 5. The weak signal intensity of 396.8 eV and 398.8 eV in Fig. 5**(a)** were assigned to Al-O-N and AlN, respectively. The low intensity of N-containing species at the surface cycled in the EC electrolyte suggests

Table 2
Mass loss percentages of Al foils in 1 M LiTFSI electrolytes using EC, EC:DEC (1:1 v/v), MPN, and EC:MPN solvents in the Al||Li corrosion test at 4.5 V and 5.0 V (vs. Li^+/Li^+).

Mass loss of holding voltage (%)	EC	EC:MPN (7:3 v/v)	EC:MPN (1:1 v/v)	EC:MPN (3:7 v/v)	MPN
5.0 V	-18.2%	-15.3%	-12.9%	-8.8%	-0.5%
4.5 V	-12.8%	-1.4%	-2.6%	-2%	-0.5%

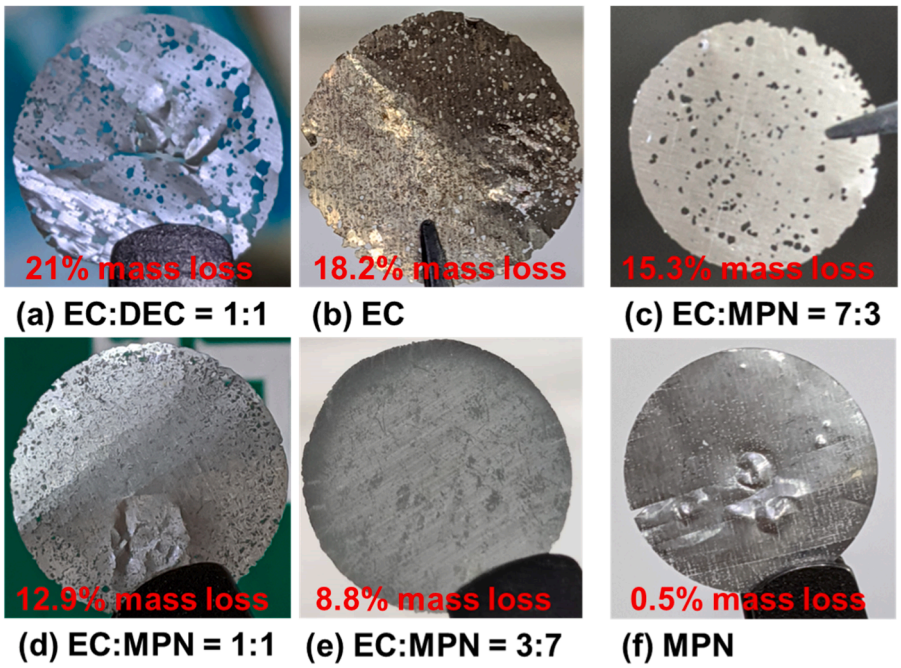

Fig. 3. Photographs and the mass loss percentage of Al foils in the Al||Li cells corrosion tests at 5 V (vs. Li^+/Li) in 1 M LiTFSI electrolytes using (a) EC:DEC 1:1 v/v, (b) EC, (c) EC:MPN 7:3 v/v, (d) EC:MPN 1:1 v/v, (e) EC:MPN 3:7 v/v, and (f) MPN solvents.

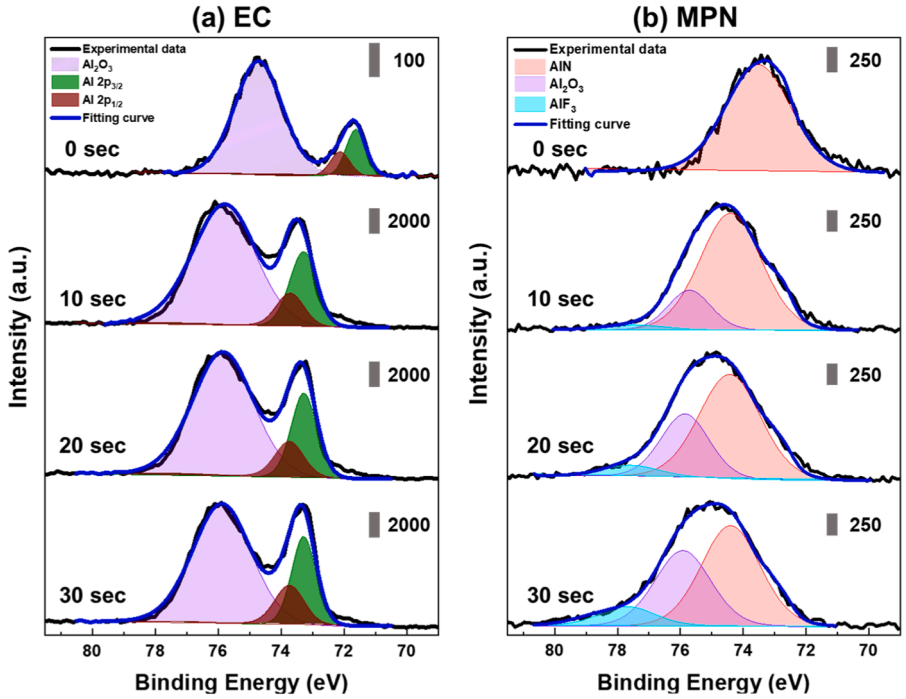

Fig. 4. Al 2p XPS spectra of the Al foils after one charge-discharge cycle in the Al||Li coin cells using 1 M LiTFSI with (a) EC and (b) MPN solvents. The spectra were collected after sputtering times of 0-30 s (intensity scale provided for each individual spectrum).

that AlN formation from the reaction between Al foil and the Li salt during cycling is limited in the EC-based formulation. Compared with the carbonate solvent, the N 1s XPS spectra of AlN and Al-O-N that formed in the MPN-based electrolyte were characterised by the more intense 396.2 eV and 398.8 eV signals on the Al foil surface, as shown in Fig. 5**(b)** [35–38]. With an increase of the sputtering time in Fig. 5**(b)**, AlN remains the dominant surface species, in agreement with the observations in the Al 2p XPS spectra in Fig. 4.

The F 1s XPS spectra for Al foils cycled in the EC and MPN formulations are presented in Fig. 6. For the 1 M LiTFSI electrolyte using EC solvent, broad peaks are observed on the XPS spectrum, which may come from the weak bonding of the fluorine species deposited on the Al surface, shown in Fig. 6**(a)**. After Ar^+ sputtering, signals at 684.3 eV, 686.1 eV, and 687.5 eV become visible and were identified as LiF, CF_2, and CF_x. When using MPN solvent, a large amount of CF_x amount was measured on the top of the Al surface, shown in Fig. 6**(b)**. After Ar^+ sputtering, LiF and CF_x were obtained at 685 eV and 688.5 eV, respectively [39–41]. Additionally, the central signal at 686.2 eV after

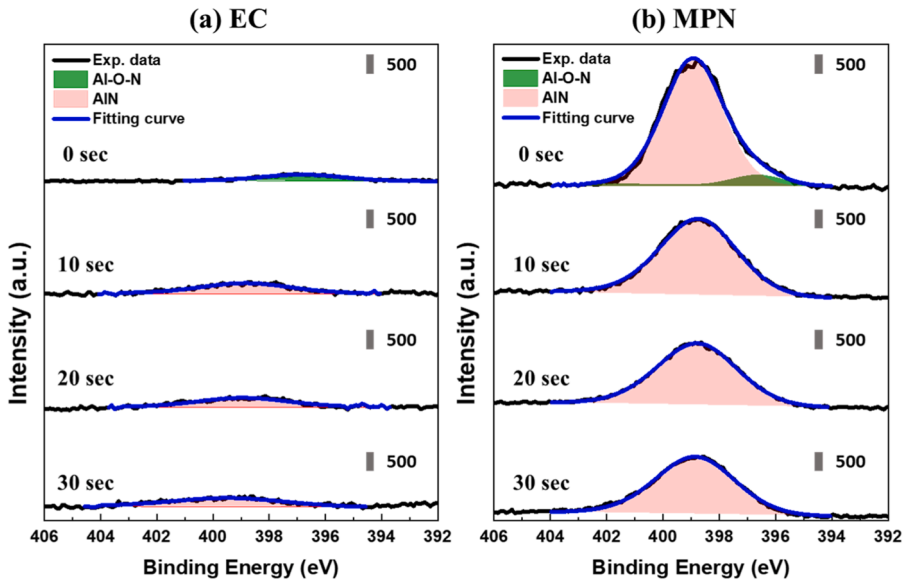

Fig. 5. N 1s XPS spectra of the Al foils after one charge-discharge cycle in the Al||Li coin cells using 1 M LiTFSI with (a) EC and (b) MPN solvents. The spectra were collected after sputtering times of 0-30 s. (Intensity scale provided for each individual spectrum).

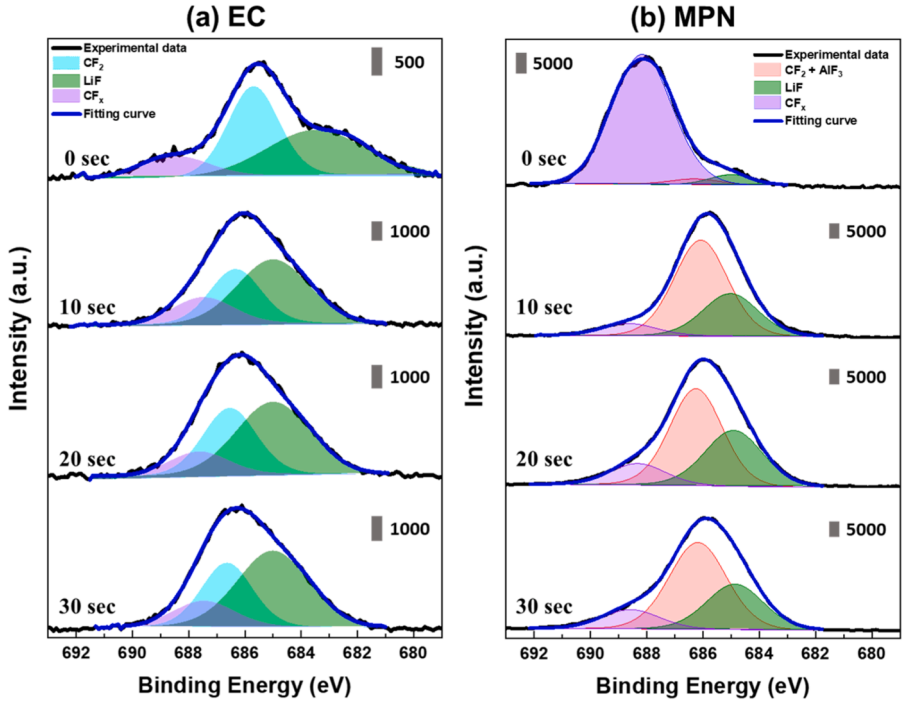

Fig. 6. F 1s XPS spectra of the aluminium foils after one charge-discharge cycle in the Al||Li coin cells using 1 M LiTFSI with (a) EC and (b) MPN solvents. The spectra were collected after sputtering times of 0-30 s. (Intensity scale provided for each individual spectrum).

sputtering was assigned to a combination of the overlapping binding energies of CF_2 and AlF_3 [42,43]. The AlF_3 character was identified earlier in the Al 2p spectra of the MPN-based electrolyte (Fig. 4**(b)**) but importantly was absent in the equivalent Al 2p spectra for the electrode cycled in EC (Fig. 4**(a)**). From these results, the formation of AlF_3 is another difference in the behaviour and functionality of the EC and MPN solvents in the 1 M LiTFSI electrolytes. Matsumoto et al. [44] also indicated that AlF_3 provided limited passivation on the aluminium surface. In this context, these results, therefore, suggest that MPN acts as a sacrificial solvent for AlN formation and AlN will play the major role in protecting the Al surface in this study. Therein, the AlN layer can act as a passivation layer on the top of the Al surface, which can inhibit the Al corrosion due to the higher pitting potential of AlN than that of Al [45]. However, given that the source of F-containing species is the TFSI anion in both formulations, these observations indicate the nature of different solvents does significantly impact the preferential oxidation pathways of the TFSI anion.

Al foils were readily corroded during the anodic treatment in 1 M LiTFSI electrolyte with EC as solvent, which is due to the absence of a passivation film on the Al surface leading to the continuous formation of $Al(TFSI)_3$, which dissolves into the carbonate solvents [46]. From the results of the Al foil corrosion tests and XPS analyses, the MPN solvent in

the electrolyte promotes the formation of an AlN-dominated film on the Al surface that, in turn, suppresses or impedes the corrosion reactions occurring at the current collector at high voltages, as shown in Fig. 7. AlN has excellent thermal conductivity and outstanding electrochemical stability against Li metal. AlN coating layers have also been shown to promote an effective stabilization of the lithium metal surface and benefit the cycle performance of the cell [47].

3.3. Cycling performance of $LiNi_{0.6}Mn_{0.2}Co_{0.2}O_2$||Li cells

To demonstrate the effectiveness of corrosion suppression in MPN-based electrolytes and the benefits for cell cycling performance, Li-ion cells using $LiNi_{0.6}Mn_{0.2}Co_{0.2}O_2$ as positive and Li metal as negative electrodes were prepared. Fig. 8 shows the charge-discharge voltage profiles of the $LiNi_{0.6}Mn_{0.2}Co_{0.2}O_2$||Li cells at a rate of 0.5C using different solvent combinations. When cycled using only the EC solvent (Fig. 8 **(a)**), the capacity dropped sharply during the first 10 cycles, which implies that significant material degradation has occurred. When the mixed solvents of EC and MPN are used in combination with LiTFSI as the electrolyte, the first cycle capacity is increased compared to the pure EC solvent. This is likely attributed in-part to the improved ionic conductivity of the EC:MPN 3:7 v/v mixed solvent electrolytes (7.9 mS cm^{-1}) compared to the electrolyte based on EC only (6.1 mS cm^{-1}). With the addition of MPN, the Al current collector in $LiNi_{0.6}Mn_{0.2}Co_{0.2}O_2$||Li cell can be passivated during cycling according to the XPS data, and the capacity retention significantly improves, benefiting cycling life, as shown in Fig. 8**(b)-8(d)**. These results demonstrate that the oxidation reaction between MPN and the Al current collectors facilitates the formation of a stable AlN passivation layer, which inhibits the significant corrosion of Al current collectors in the LiTFSI-containing electrolytes.

The cycling performance of $LiNi_{0.6}Mn_{0.2}Co_{0.2}O_2$||Li cells between 3.0 V and 4.3 V *vs.* Li/Li^+ in various 1 M LiTFSI electrolyte formulations is presented in Fig. 9**(a)**. For the formulation using only EC solvent, the cell delivers a lower initial discharge capacity of 145 mAh g^{-1} compared to the other studied electrolytes. In addition, the specific capacity of $LiNi_{0.6}Mn_{0.2}Co_{0.2}O_2$||Li cell fades drastically in the 1 M LiTFSI/EC electrolyte, decreasing from 145 to 7 mAh g^{-1} after 30 cycles. However, with the addition of MPN into 1 M LiTFSI electrolytes, the cycling life and capacity of the $LiNi_{0.6}Mn_{0.2}Co_{0.2}O_2$||Li cell are improved significantly. Therein, the $LiNi_{0.6}Mn_{0.2}Co_{0.2}O_2$||Li cells deliver increased initial capacities with increasing the MPN concentration in the EC:MPN formulations, delivering 158, 159 to 163 mAh g^{-1} for 7:3 v/v, 1:1 v/v, and 3:7 v/v, respectively. Furthermore, the capacity retention follows the same trend, wherein capacities of 45, 74 and 105 mAh g^{-1} were delivered after 60 cycles for the 7:3 v/v, 1:1 v/v, and 3:7 v/v (EC:MPN) formulations, respectively. The coulombic efficiency of the cell using the EC:MPN (3:7 v/v) solvents remains at 98.6% during cycling, which is considerably higher than 58.5% of the cell employing the formulation containing only the EC solvent. The MPN-based electrolytes also considerably outperform the EC:DMC-based LiTFSI electrolyte. This comparison confirms that the worse performance of the carbonate-only EC/LiTFSI electrolyte is not due to the worse transport properties of this formulation since the conductivity of the EC:DMC formulation (9.3 mS cm^{-1}) is comparable to the EC:MPN formulation [48]. Thus, the instability therein can be attributed to the corrosion reactions occurring in the absence of the protective layer observed when MPN is not present.

After cycling, the extreme corrosion and pitting of the Al current collector were observed in the LiTFSI/EC electrolyte (Fig. 9**(b)**). Conversely, for the cell containing the largest proportion of MPN within the electrolyte formulation, the corrosion was dramatically reduced, with minimal visible damage to the Al metal surface following these testing parameters, shown in Fig. 9**(c)**. The formulation 1 M LiTFSI EC:MPN (3:7 v/v) performs closest (blue triangles) to the baseline capacity of ca. 160 mAh g^{-1} (black triangles) achieved with the benchmark electrolyte of 1 M $LiPF_6$ in EC:DMC (1:1 v/v). The performance of these cells indicated that the degradation could be due to the lack of a passivation film on the Al current collector in the LiTFSI/EC electrolyte, and the better cycling performance is attributed to the formation of an AlN protective layer when MPN solvent is added into the electrolyte.

4. Conclusions

In this work, the physical and electrochemical properties of 1 M LiTFSI electrolytes using ethylene carbonate (EC) and 3-methoxypropionitrile (MPN) solvents were characterised. The onset corrosion potential of the aluminium (Al) current collector increased from 3.67 V to 4.21 V (*vs.* Li^+/Li) in the 1 M LiTFSI electrolyte with increasing the volume ratio of MPN with respect to EC. As the amount of MPN solvent increased, the anodic stability for Al electrodes was found to be improved in the electrolyte based on the LiTFSI salt and the corrosion of Al was considerably suppressed. Importantly, the addition of the MPN solvent results in the formation of a dominant aluminium nitride surface layer that helps stabilise the current collector interface at highly positive potentials, as determined by XPS. In addition, in the $LiNi_{0.6}Mn_{0.2}Co_{0.2}O_2$||Li cell using the 1 M LiTFSI-EC electrolyte, severe corrosion of the Al current collector could contribute to the accelerated capacity loss of these cells and failure after only 10 cycles. However, the capacity retention was significantly enhanced when using EC:MPN (3:7 v/v) with 1 M LiTFSI as the electrolyte formulation, delivering *ca.* 75% of the initial 160 mAh g^{-1} after 60 cycles. This highlights the beneficial effect of MPN leading to the stabilisation of the Al interface during cycling in the presence of LiTFSI.

CRediT authorship contribution statement

Chih-Han Yen: Conceptualization, Methodology, Writing – original draft, Formal analysis, Data curation. **Alex R. Neale:** Methodology, Investigation, Data curation, Writing – review & editing. **Jungwoo Lim:** Data curation, Writing – review & editing. **Dominic Bresser:** Resources, Writing – review & editing. **Laurence J. Hardwick:** Writing – review & editing, Supervision. **Chi-Chang Hu:** Writing – review & editing, Supervision.

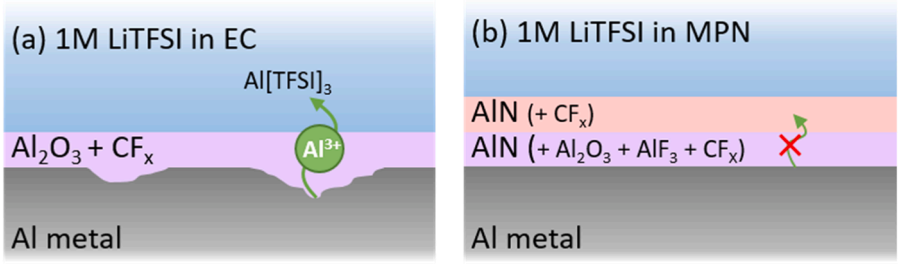

Fig. 7. Schematic of (a) Al corrosion in 1 M LiTFSI/EC and (b) an AlN passivation film formation in 1 M LiTFSI/MPN in the Al||Li cell as determined from XPS analysis.

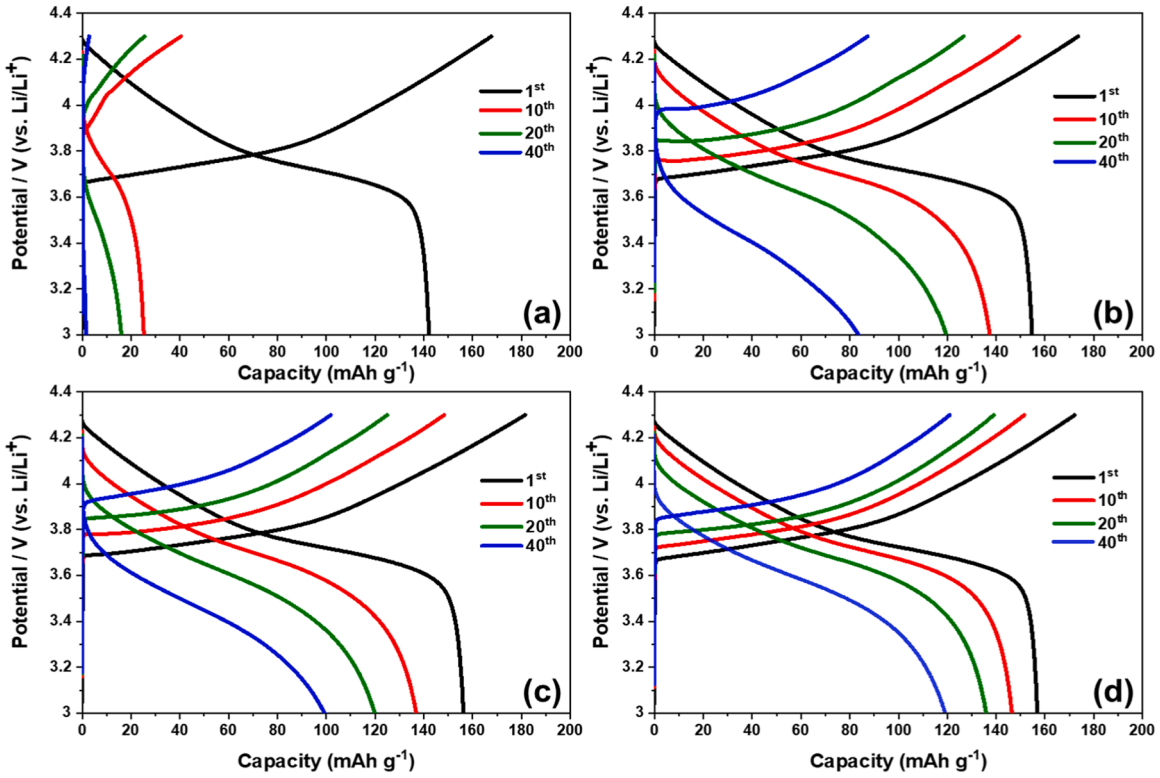

Fig. 8. Charge-discharge curves of $LiNi_{0.6}Mn_{0.2}Co_{0.2}O_2$ ||Li half cells in 1 M LiTFSI electrolytes with (a) EC, (b) EC:MPN 7:3 v/v, (c) EC:MPN 1:1 v/v, and (d) EC:MPN 3:7 v/v with first cycle at 0.1 C and the remaining cycles at 0.5 C.

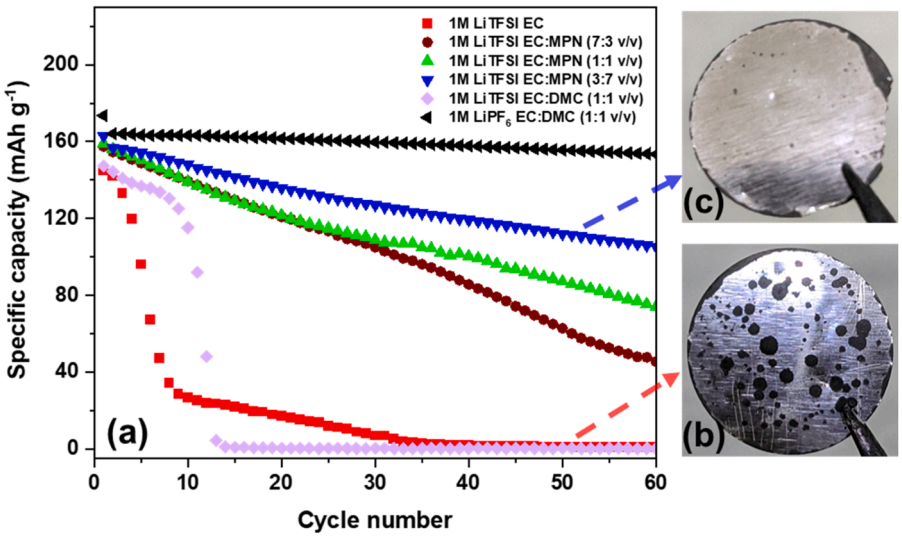

Fig. 9. (a) Cycling performance of $LiNi_{0.6}Mn_{0.2}Co_{0.2}O_2$||Li half cells in 1 M LiTFSI-based electrolytes, and optical images of the Al current collectors after cycling in the (b) EC and (c) EC:MPN (3:7 v/v) based electrolytes. The cells were cycled at 0.1C for the first cycle, then at 0.5 C for the remaining cycles.

Declaration of Competing Interest

The authors declare that they have no known competing financial interests or personal relationships that could have appeared to influence the work reported in this paper

Data Availability

Data will be made available on request.

Acknowledgments

ARN acknowledges funding from EPSRC funding for the project Earth-Abundant Metal-Air Batteries (EP/R020744/1) and JL support from the Faraday Institution Project CATMAT (EP/S003053/1, FIRG016). XPS data collection was performed at the EPSRC National Facility for XPS ("HarwellXPS"), operated by Cardiff University and UCL, under contract No. PR16195, and Dr. Mark Isaacs. Dr. Hatem Amli and Prof. Vin Dhanak are acknowledged for facilitating the XPS measurements. The financial support of this work conducted in Taiwan, by

the Ministry of Science and Technology (MOST) of Taiwan under contract no. MOST 109-2923-E-007-005 and 110-2923-E-007-011, is gratefully acknowledged. Moreover, financial support from the German Ministry of Education and Research (BMBF) within the HighSafe-2 project (03XP0306C) is gratefully acknowledged.

References

[1] N.S. Choi, Z. Chen, S.A. Freunberger, X. Ji, Y.K. Sun, K. Amine, G. Yushin, L. F. Nazar, J. Cho, P.G. Bruce, Challenges facing lithium batteries and electrical double-layer capacitors, Angew. Chem. Int. Ed. 51 (2012) 9994–10024.
[2] J.B. Goodenough, Y. Kim, Challenges for rechargeable Li batteries, Chem. Mater. 22 (2010) 587–603.
[3] B. Scrosati, J. Hassoun, Y.-K. Sun, Lithium-ion batteries. A look into the future, Energy Environ. Sci. 4 (2011) 3287–3295.
[4] M. Armand, J.M. Tarascon, Building better batteries, Nature 451 (2008) 652–657.
[5] Y. Tian, G. Zeng, A. Rutt, T. Shi, H. Kim, J. Wang, J. Koettgen, Y. Sun, B. Ouyang, T. Chen, Promises and challenges of next-generation "beyond Li-ion" batteries for electric vehicles and grid decarbonization, Chem. Rev. 121 (2020) 1623–1669.
[6] J. Ma, Y. Li, N.S. Grundish, J.B. Goodenough, Y. Chen, L. Guo, Z. Peng, X. Qi, F. Yang, L. Qie, The 2021 battery technology roadmap, J. Phys. D Appl. Phys. 54 (2021), 183001.
[7] K. Kanamura, H. Takezawa, S. Shiraishi, Z.I. Takehara, Chemical reaction of lithium surface during immersion in LiClO4 or LiPF6/DEC electrolyte, J. Electrochem. Soc. 144 (1997) 1900.
[8] H. Yang, G.V. Zhuang, P.N. Ross, Thermal stability of LiPF6 salt and Li-ion battery electrolytes containing LiPF6, J. Power Sources 161 (2006) 573–579.
[9] G. Zhou, X. Sun, Q.H. Li, X. Wang, J.N. Zhang, W. Yang, X. Yu, R. Xiao, H. Li, Mn ion dissolution mechanism for lithium-ion battery with LiMn2O4 cathode: *in situ* ultraviolet–visible spectroscopy and Ab Initio molecular dynamics simulations, J. Phys. Chem. Lett. 11 (2020) 3051–3057.
[10] C. Lin, A. Tang, H. Mu, W. Wang, C. Wang, Aging mechanisms of electrode materials in lithium-ion batteries for electric vehicles, J. Chem., 2015 (2015).
[11] Z. Lu, L. Yang, Y. Guo, Thermal behavior and decomposition kinetics of six electrolyte salts by thermal analysis, J. Power Sources 156 (2006) 555–559.
[12] S.F. Lux, L. Terborg, O. Hachmöller, T. Placke, H.W. Meyer, S. Passerini, M. Winter, S. Nowak, LiTFSI stability in water and its possible use in aqueous lithium-ion batteries: ph dependency, electrochemical window and temperature stability, J. Electrochem. Soc. 160 (2013) A1694–A1700.
[13] E. Cho, J. Mun, O.B. Chae, O.M. Kwon, H.-T. Kim, J.H. Ryu, Y.G. Kim, S.M. Oh, Corrosion/passivation of aluminum current collector in bis (fluorosulfonyl) imide-based ionic liquid for lithium-ion batteries, Electrochem. Commun. 22 (2012) 1–3.
[14] D. Di Censo, I. Exnar, M. Graetzel, Non-corrosive electrolyte compositions containing perfluoroalkylsulfonyl imides for high power Li-ion batteries, Electrochem. Commun. 7 (2005) 1000–1006.
[15] A. Mauger, C. Julien, A. Paolella, M. Armand, K. Zaghib, A comprehensive review of lithium salts and beyond for rechargeable batteries: progress and perspectives, Mater. Sci. Eng. R: Rep. 134 (2018) 1–21.
[16] M.S. Park, S.B. Ma, D.J. Lee, D. Im, S.G. Doo, O. Yamamoto, A highly reversible lithium metal anode, Sci. Rep. 4 (2014) 1–8.
[17] B. Pohl, M. Grünebaum, M. Drews, S. Passerini, M. Winter, H.D. Wiemhöfer, Nitrile functionalized silyl ether with dissolved LiTFSI as new electrolyte solvent for lithium-ion batteries, Electrochim. Acta 180 (2015) 795–800.
[18] Y. Abu-Lebdeh, I. Davidson, New electrolytes based on glutaronitrile for high energy/power Li-ion batteries, J. Power Sources 189 (2009) 576–579.
[19] D. Farhat, D. Lemordant, J. Jacquemin, F. Ghamouss, Alternative electrolytes for Li-Ion batteries using glutaronitrile and 2-methylglutaronitrile with lithium bis (trifluoromethanesulfonyl) imide, J. Electrochem. Soc. 166 (2019) A3487.
[20] H. Duncan, N. Salem, Y. Abu-Lebdeh, Electrolyte formulations based on dinitrile solvents for high voltage Li-ion batteries, J. Electrochem. Soc. 160 (2013) A838.
[21] I. Cekic-Laskovic, N. von Aspern, L. Imholt, S. Kaymaksiz, K. Oldiges, B.R. Rad, M. Winter, Synergistic effect of blended components in nonaqueous electrolytes for lithium ion batteries, Top. Curr. Chem. 375 (2017) 1–64.
[22] E. Krämer, S. Passerini, M. Winter, Dependency of aluminum collector corrosion in lithium ion batteries on the electrolyte solvent, ECS Electrochem. Lett. 1 (2012) C9.
[23] J. Garche, C. Dyer, P.T. Moseley, Z. Ogumi, D.A. Rand, B. Scrosati, Encyclopedia of electrochemical power sources, Newnes (2013).
[24] S. Hess, M. Wohlfahrt-Mehrens, M. Wachtler, Flammability of Li-ion battery electrolytes: flash point and self-extinguishing time measurements, J. Electrochem. Soc. 162 (2015) A3084–A3097.
[25] Q. Wang, S.M. Zakeeruddin, I. Exnar, M. Grätzel, 3-Methoxypropionitrile-based novel electrolytes for high-power Li-ion batteries with nanocrystalline Li_4Ti_5 O 12 Anode, J. Electrochem. Soc. 151 (2004) A1598.
[26] N. Fairley, A. Carrick, N. Fairly, The Casa Cookbook, Acolyte Sci. Cheshire (2005).
[27] J. Garche, C.K. Dyer, P.T. Moseley, Z. Ogumi, D.A. Rand, B. Scrosati, Encyclopedia of electrochemical power sources, Newnes (2013).
[28] S. Hess, M. Wohlfahrt-Mehrens, M. Wachtler, Flammability of Li-ion battery electrolytes: flash point and self-extinguishing time measurements, J. Electrochem. Soc. 162 (2015) A3084.
[29] P. Isken, C. Dippel, R. Schmitz, R. Schmitz, M. Kunze, S. Passerini, M. Winter, A. Lex-Balducci, High flash point electrolyte for use in lithium-ion batteries, Electrochim. Acta 56 (2011) 7530–7535.
[30] X. Zhang, T. Devine, Factors that influence formation of AlF3 passive film on aluminum in Li-ion battery electrolytes with LiPF6, J. Electrochem. Soc. 153 (2006) B375.
[31] G.P. Gakis, C. Vahlas, H. Vergnes, S. Dourdain, Y. Tison, H. Martinez, J. Bour, D. Ruch, A.G. Boudouvis, B. Caussat, Investigation of the initial deposition steps and the interfacial layer of atomic layer deposited (ALD) Al2O3 on Si, Appl. Surf. Sci. 492 (2019) 245–254.
[32] J. Mun, T. Yim, C.Y. Choi, J.H. Ryu, Y.G. Kim, S.M. Oh, Linear-sweep thermammetry study on corrosion behavior of Al current collector in ionic liquid solvent, Electrochem. Solid State Lett. 13 (2010) A109.
[33] G. Greczynski, L. Hultman, Towards reliable X-ray photoelectron spectroscopy: Sputter-damage effects in transition metal borides, carbides, nitrides, and oxides, Appl. Surf. Sci. 542 (2021), 148599.
[34] W. Egelhoff Jr, Core-level binding-energy shifts at surfaces and in solids, Surf. Sci. Rep. 6 (1987) 253–415.
[35] J. Caicedo, J. Pérez, H. Caicedo, H. Riascos, Determination of physical response in (Mo/AlN) SAW devices, Surf. Rev. Lett. 20 (2013), 1350017.
[36] K. Lawniczak-Jablonska, Z. Zytkiewicz, S. Gieraltowska, M. Sobanska, P. Kuzmiuk, K. Klosek, Chemical bonding of nitrogen formed by nitridation of crystalline and amorphous aluminum oxide studied by X-ray photoelectron spectroscopy, RSC Adv. 10 (2020) 27932–27939.
[37] P. Motamedi, K. Cadien, XPS analysis of AlN thin films deposited by plasma enhanced atomic layer deposition, Appl. Surf. Sci. 315 (2014) 104–109.
[38] C. Ozgit-Akgun, E. Goldenberg, A.K. Okyay, N. Biyikli, Hollow cathode plasma-assisted atomic layer deposition of crystalline AlN, GaN and Al x Ga 1 x N thin films at low temperatures, J. Mater. Chem. C 2 (2014) 2123–2136.
[39] L. Cong, J. Liu, M. Armand, A. Mauger, C.M. Julien, H. Xie, L. Sun, Role of perfluoropolyether-based electrolytes in lithium metal batteries: Implication for suppressed Al current collector corrosion and the stability of Li metal/electrolytes interfaces, J. Power Sources 380 (2018) 115–125.
[40] D. Ensling, M. Stjerndahl, A. Nytén, T. Gustafsson, J.O. Thomas, A comparative XPS surface study of Li 2 FeSiO 4/C cycled with LiTFSI-and LiPF 6-based electrolytes, J. Mater. Chem. 19 (2009) 82–88.
[41] S. Leroy, H. Martinez, R. Dedryvère, D. Lemordant, D. Gonbeau, Influence of the lithium salt nature over the surface film formation on a graphite electrode in Li-ion batteries: an XPS study, Appl. Surf. Sci. 253 (2007) 4895–4905.
[42] H. Sun, P. Liang, G. Zhu, W.H. Hung, Y.Y. Li, H.C. Tai, C.L. Huang, J. Li, Y. Meng, M. Angell, A high-performance potassium metal battery using safe ionic liquid electrolyte, Proc. Natl. Acad. Sci. 117 (2020) 27847–27853.
[43] C.T. Chu, A. Mondal, N.V. Kosova, J.Y. Lin, Improved high-temperature cyclability of AlF3 modified spinel $LiNi_{0.5}Mn_{1.5}O_4$ cathode for lithium-ion batteries, Appl. Surf. Sci. 530 (2020), 147169.
[44] K. Matsumoto, K. Inoue, K. Nakahara, R. Yuge, T. Noguchi, K. Utsugi, Suppression of aluminum corrosion by using high concentration LiTFSI electrolyte, J. Power Sources 231 (2013) 234–238.
[45] H. Schäfer, H.R. Stock, Improving the corrosion protection of aluminium alloys using reactive magnetron sputtering, Corros. Sci. 47 (2005) 953–964.
[46] M. Morita, T. Shibata, N. Yoshimoto, M. Ishikawa, Anodic behavior of aluminum in organic solutions with different electrolytic salts for lithium ion batteries, Electrochim. Acta 47 (2002) 2787–2793.
[47] P.J.H. Kim, V.G. Pol, Surface functionalization of a conventional polypropylene separator with an aluminum nitride layer toward ultrastable and high-rate lithium metal anodes, ACS Appl. Mater. Interfaces 11 (2019) 3917–3924.
[48] M. Dahbi, F. Ghamouss, F. Tran-Van, D. Lemordant, M. Anouti, Comparative study of EC/DMC LiTFSI and LiPF6 electrolytes for electrochemical storage, J. Power Sources 196 (2011) 9743–9750.